Shear Modulus of Cylindrical CFRP Tendons Exposed to Moisture

Eleni Toumpanaki[1], Janet M. Lees[2], Giovanni P. Terrasi[3]

Abstract

Two groups of cylindrical CFRP tendons were exposed in distilled water at 23°C and 60°C to study the diffusion mechanisms and the effect of moisture uptake on the tendon shear modulus. The two tendon groups had different manufacturing processes, so DMA tests and optical microscopy were used to help characterise the materials. Mass uptake readings of tendon samples were recorded and the uptake generally agreed with Fickian predictions. To study the time-dependent changes in the matrix stiffness due to exposure, torsion tests within the elastic range of loading were conducted. The tendon shear modulus was then derived from the torque versus twist plots. For both groups of tendons the measured shear modulus decreased due to exposure in water. A long-term shear modulus prediction model was developed to relate the tendon torsional shear stiffness and the moisture concentration and the results appeared to agree well with the experimental findings.

Author Keywords: Carbon fiber reinforced polymer, Durability, Prediction model

[1]Ph.D. Candidate, Department of Engineering, University of Cambridge, Trumpington Street, Cambridge, UK, CB2 1PZ, Tel: +44(0)12233 32758, e-mail: et343@cam.ac.uk (corresponding author)

[2]Reader in Civil Engineering, Department of Engineering, University of Cambridge, Trumpington Street, Cambridge, UK, CB2 1PZ, e-mail: jmL2@eng.cam.ac.uk

[3]Head, Laboratory for Mechanical Systems Engineering, Swiss Federal Laboratories for Materials Science and Technology (EMPA), Überlandstrasse 129, 8600 Dübendorf, Switzerland, e-mail: giovanni.terrasi@empa.ch

Introduction

Recent high-profile incidents of the corrosion of steel reinforcement in prestressed concrete bridge structures, e.g. the Mid Bay Bridge in Florida (Hartt and Venugopalan 2002) and Hammersmith Flyover Bridge in London (Lynch 2012), have exemplified the extensive disruption and costs associated with steel corrosion. The use of fibre reinforced polymer (FRP) tendons as internal concrete reinforcement is a proactive means to avoid chemical corrosion. Despite their high initial cost, FRP tendons can be effective in terms of the whole life costing of a structure and the full strain capacity can be exploited if the tendons are prestressed (Burgoyne and Balafas 2007). However, a lack of confidence in the adoption of new structural materials has limited the wider field applications of FRPs. Moreover, the long term durability of FRPs in wet environments remains an area of active research. It is important to ensure that FRP tendons are not adversely affected due to moisture absorption in the resin matrix material.

To date, design guidelines and codes for concrete reinforced with carbon FRP (CFRP) have proposed strength reduction factors for environmental exposure, but due to the complexities of the interactions there can be a lack of a firm experimental or analytical basis to support these recommendations (Huang and Aboutaha 2010). Furthermore, the strength reduction factors tend to relate to fibre dominated properties, such as tensile strength (ACI 2006), but do not necessarily reflect matrix dominated properties, such as the bond performance, shear strength, dowel strength and creep, all of which can be degraded from exposure in wet environments. Another factor not explicitly considered by standards is the manufacturing process of the CFRP tendons and in particular the curing (Krishna et al. 2010).

Manufacturing process in CFRP tendons

The most suitable manufacturing process for cylindrical FRP bars used as prestressing tendons is the pultrusion method. Pultrusion offers a high speed of production for constant circular cross sections with high fibre volume fractions. The resulting bars have a high stiffness through the alignment of unidirectional fibres (Mayer 1996). The final quality of the CFRP tendons is regulated by a low void percentage and a high crosslinking density of the epoxy matrix.

The die length and temperature, the pull out speed and the heat power input influence both the presence and percentage of voids in pultruded FRPs (Li et al. 2002; Lam et al. 2003). The fibre sizing, coupling agent and resin viscosity also play a role (Kelly 1989). The effect of the void content has been mainly studied in aerospace engineering, since increased porosity has been reported in laminate structures. This most commonly occurs in the resin rich interface layers as a result of the lay-up manufacturing process. Voids have a greater effect on the interlaminar shear (ILSS) and flexural strength than on the tensile modulus and strength (Olivier et al. 1995; Liu et al. 2006). This is because pores replace the matrix material and develop preferentially in the fibre-matrix interface. Even for the same absolute void percentage large variations in performance have been reported due to a dependency on the width to length aspect ratio of the voids (Huang and Talreja 2005; Zhu et al. 2009). Hancox (1977) reported a 70% decrease in shear modulus and strength of wet moulded CFRP rods with a 5% void content and observed that interconnected void regions enable the shear crack paths to initiate and develop. Zhu et al. (2009) recorded a drop of up to 16% in the ILSS of carbon/epoxy laminates with 8% porosity relative to laminates with 0.2% porosity.

The curing temperature and curing time in the manufacturing process controls the degree of molecular crosslinking in a resin matrix and consequently influences the chemical stability and mechanical performance on the macroscale. The polymerisation of epoxy groups is the result of three principal curing reactions. The first curing reaction is between an epoxide group and the primary amine group of the curing agent. The second reaction has a lower rate and a second curing run is often required for the full conversion of the secondary amines (Vanlandingham et al. 1999a). The etherification of the remaining unreacted and reacted epoxy groups is the final stage of the curing process and takes place only at high temperatures and longer times (Vanlandingham et al. 1999a) or in the presence of catalysts (Wu 1992) . In practice the experimental detection of the degree of crosslinking in epoxies is difficult and consequently the molecular structure and mechanical properties cannot be directly related. The most commonly used methods to infer the crosslinking density are by determining the glass transition temperature (T_g) values using Dynamic Mechanical Analysis (DMA) (e.g. Vanlandingham et al. 1999a) and Differential Scanning Calorimetry (DSC) (e.g. Wu 1992) . A higher crosslinking density is believed to result in a higher T_g value (Wu 1992; Vanlandingham et al. 1999a).

Exposure to moisture

In humid environments, the matrix component of a CFRP tendon is the main source of degradation, since carbon fibres are generally considered to be impermeable due to their highly aligned and crystalline structure. The moisture diffusion process in epoxies is governed by two factors. The first is the availability of molecular sized holes (free volume) which is inherently dependent on the crosslinking density (Diamant et al. 1981; Vanlandingham et al. 1999b) and hence on the hardener type and extent of cure (Diamant et al. 1981; Wright 1981). This process is reversible upon drying. The second factor is the

hydrogen bonding of the water molecules in the sorption sites in the polymer such as the hydroxyl groups (bound molecules). This process is irreversible and leads to the swelling of the epoxy matrix material (Adamson 1980). The water uptake in epoxies is also affected by a number of other parameters including the polymer polarity, unreacted amine groups, and the development of a two phase structure (Diamant et al. 1981). All these factors are related to the manufacturing variables, such as the stoichiometry, mixing conditions, temperature, extent of cure and pressure. A decrease in the diffusivity of epoxy systems (Marais et al. 2000) and the water saturation levels in CFRPs (Ankara et al. 1986) have been attributed to a higher degree of cure and additional crosslinking. However, Min et al. (1993) have found that additional crosslinking does not necessarily result in a lower diffusivity.

Accelerated ageing can be used to obtain long-term data from short exposure times. The most widely accepted method based on the Arrhenius principles is to accelerate moisture uptake with the application of elevated temperatures in conjunction with exposure in humid environments. It is assumed that one chemical degradation mechanism exists and accelerates by elevating the temperature. However, longer exposure times and longer exposure temperatures may cause hydrolysis resulting in mass loss. In general, CFRP tendons exhibit a good chemical resistance against hydrolysis (chain scission) due to the stability of the epoxy resin and carbon fibres when subjected to wet environments. Nevertheless, hydrolysis has been observed in epoxy matrices exposed in distilled water at high temperatures near the glass transition temperature of the exposed sample (Xiao and Shanahan 1997). Therefore, the temperature applied should be much lower than the T_g value of the unexposed epoxy to avoid additional degradation mechanisms that are not representative. However, moisture absorption decreases the T_g of the epoxies and hence a

safe threshold should be defined. Dolan et al. (2008) suggested that an elevated exposure temperature should be at least 15°C lower than the T_g value. However, a reduction in T_g of up to 30°C has been reported in a CFRP laminate exposed at 95% RH and 50°C for 1.7% moisture uptake and with a reference T_g value of 135°C (Birger et al. 1989). Furthermore, Robert et al. (2010) observed additional degradation mechanisms in GFRP bars immersed in distilled water at 80°C, even though the T_g of an unexposed specimen was 96°C. According to ACI (2006), 60°C is recommended as an accelerated ageing temperature for structural FRP materials.

Effect of moisture on strength and stiffness

A common test method to assess the long-term durability of matrix dominated properties in FRPs is the short beam test method. This method can provide insight into both the stiffness and strength implications of moisture exposure. In the context of a matrix strength assessment, the test is more directly applicable to laminate structures, where the failure takes place mostly between laminas and so the interlaminar shear stress (ILSS) can be derived. In durability tests on unidirectional carbon/epoxy laminates manufactured with a wet lay-up method, Abanilla et al. (2006) reported a 33.4% reduction in interlaminar shear strength after 100 weeks of exposure in alkaline solution and a 20% reduction in interlaminar shear modulus after 100 weeks of exposure in deionised water at 23°C. Interlaminar shear strength reductions in CFRP rods of 14-35% have been reported after exposure in alkali solution at 60°C for 42 days (Micelli and Nanni 2001). Scott and Lees (2012) conducted short beam shear tests on CFRP tendons that had been immersed in either water (W), salt water (SW) or concrete pore solution (CPS) for roughly 1.5 years at 60 °C. For specimens without axial stress loaded transversely with flat plates, the ultimate shear load of the SW and W specimens did not differ significantly from the unexposed

control samples but a 7% loss of strength was noted after CPS exposure. The average measured stiffnesses of the exposed tendons were less than the unexposed samples and, for example, the load versus deflection slope for the water-exposed samples was around 30% lower at small displacements. Transverse shear tests on CFRP tendons using rounded plates were also conducted. However, it was postulated that the inference of the matrix strength from the peak load may result in misleading conclusions since in these tests the failure process can shift from a matrix-dominated to fiber-dominated mechanism (Scott and Lees, 2012). Such fiber-dominated effects also have ramifications for the measured matrix stiffness. Scott and Lees (2012) noted three stages of behaviour from the rounded plate load deflection results. The first stage at small displacements was felt to be the most representative of the matrix stiffness. The tendons then delaminated which led to a second phase of behavior associated with further delamination and an increase in displacement under constant load. A final phase, after large displacements, was characterized by a stiffer response associated with fiber-stiffening mechanisms. In short beam tests on GFRP rods, Chen et al. (2007a) observed a lower slope in the load versus deflection plots for deflections up to 0.5 mm and attributed this to the low matrix strength and stiffness. But the slope then increased with increasing load up to failure.

Torsion testing

To study changes in matrix stiffness due to moisture exposure and to mitigate the fibre stiffening mechanisms prevalent in short beam shear tests, the current work investigates the testing of CFRP rods in torsion. In a torsion test, the shear modulus of an FRP rod, in a plane perpendicular to the fibre direction, can be measured while minimising stress concentrations and normal bending stresses. Studies on the torsional mechanical behaviour of CFRP rods (Hancox 1972; Hiermer et al. 1998) and laminates (Ogasawara et al. 2007)

have been carried out, but have primarily focused on the elastic-plastic behaviour and the ultimate strength properties. For cylindrical tendons, the stiffness of the epoxy matrix can be derived from the torsional shear modulus values and at small rotations fibre stiffening effects are minimised. A further advantage is that, after exposure, the moisture uptake occurs first in the outer perimeters of the CFRP cross-section. In a torsion test, it is the outer perimeter where the maximum torsional shear stresses act and contribute most to the shear stiffness. Therefore, any degradation of these regions can be observed after relatively short exposure times. CFRP tendons, produced using two different manufacturing methods, are studied. To characterise the tendon moisture uptake properties, the diffusion behaviour is studied with short tendon samples immersed in water at 23°C and 60°C. CFRP tendons are tested elastically in torsion after different exposure times to investigate the relationship between the moisture uptake and shear modulus degradation. A model relating the radial diffusion to the change in shear modulus is developed to predict the shear modulus degradation with time.

Experimental Program

Materials

The CFRP tendons used in this research are categorised into two groups C and D, based on their manufacturing details. Both groups of tendons had the same Bakelite EPR 4434 epoxy and EPH 943 hardener, Tenax UTS 5631 fibres and fibre volume fraction, V_f=64%. However, the nominal tendon diameters differed and were 4.2 mm and 5.4 mm for groups C and D respectively. These values refer to the nominal diameter of the core tendon as provided by the manufacturer and were adopted in the following calculations. The core diameters of both groups C and D tendons were also measured with a micrometer and

found to be Φ=4.15 ±0.06 mm and Φ=5.44 ±0.014 mm respectively. The group C tendons were manufactured specifically for research purposes and were uncoated. In contrast, the group D specimens were commercial products and so had a sand coating layer to improve the bond between the tendon and concrete. This means that there was an additional in-line production step during pultrusion, where an additional epoxy layer was applied, sand particles were sprayed and further curing followed. For this experimental series the sand coating layer was gently scraped off with a sharpened blade from the group D CFRP tendons. The exact details of the cure cycle are confidential but during the curing process the group C and D tendons were heated to a maximum temperature of 195°C.

Material characterization: Optical Microscopy and DMA tests

To verify the quality of the manufacture, the fibre size and the fibre-matrix interface, samples were studied using a Leica DMLM Optical Microscope (Leica Microsystems, Germany). Unexposed tendon samples were cut with a Dremel 398 tool (Dremel Europe, UK) and cast into a resin matrix (Acri-kleer cold mounting). The samples were later polished with P800 (22 μm) and P400 (5 μm) abrasive silicon paper.

Dynamical Mechanical Analysis (DMA) tests were conducted to measure the T_g values of the CFRP tendons and to infer the crosslinking density of the epoxy, since these two properties are felt to be interrelated (Min et al. 1993; Vanlandingham et al. 1999a). Two samples from group C (C_1 & C_2) and one sample from group D (D_1) were tested. The number of the tested specimens is limited and not sufficient for a full statistical analysis. Nonetheless, the DMA results can help to identify fundamental differences between the two tendon groups. The specimens were 40 mm long and were machined to square sections of 3.10mm × 3.10 mm for group C and 3.60 mm × 3.60 mm for group D. The

dimensions varied at most by 1% along the length of the specimens. All specimens were preconditioned at 23°C ± 2°C and RH = 50% ± 5 % for at least 7 days before testing in a 3 point bending mode. The ramp rate was 2°C/min, the frequency was fixed at 10 Hz, the temperature ranged from 23°C – 210°C and strain amplitude of 0.02 mm was applied. The T_g values were measured from the peak of the tanδ plot.

Exposure and moisture absorption

A number of 100 mm tendon samples were immersed for moisture absorption tests, where the mass weight was recorded at different times. Five 100mm length CFRP samples from both groups C and D were fully immersed in distilled water in separate polypropylene containers and were stored in the lab at room temperature (23°C). In addition, four immersed samples from group C and two samples from group D were stored in the oven at 60°C to accelerate the ageing process. The 60°C exposure conditions are well below the measured T_g values of the epoxy used (see next section) and so this temperature was unlikely to invoke unrepresentative degradation mechanisms. The mass uptake in the 100 mm samples was regularly recorded using an Oertling R20 (Oertling Ltd, UK) analogue balance machine with a 0.0001 g resolution. Before each measurement the specimens were blotted dry with a tissue paper and left at room temperature for 5 min. The average of three separate mass readings was recorded as the mass weight at a given time.

Torsion rig and torsion testing procedure

The torsion rig set-up is shown in Figure 1a. The torsion tests were carried out according to ASTM E143-02. One end of a 300 mm long tendon is gripped in a three jaw chuck, while the other end is free to twist. At the right hand support, a fixed bearing enables axial

movement through a long recess which extends beyond the length required to support the tendon (Figure 1b). A perpendicular lever arm is attached to the tendon using the clamp shown in Figure 1c. A rubber layer is inserted between the tendon and the clamp to enhance the friction and avoid slipping. A spirit level fixed on the lever arm ensures the tendon is correctly aligned before testing. Loading weights of 50 g are applied to the lever arm through a wire. The torque was calculated as the load multiplied by the lever arm (162 mm) but was corrected for the change in the angle of the lever arm. Inclinometers with a range -15˚ to 15˚ and with a 0.0006˚ resolution measured the rotation of the specimens. The inclinometers were calibrated before every torsion test and the resulting calibration factors were validated against a specified nominal range. Each inclinometer is attached through a mounting plate to a hexagonal section at the midpoint of the inclinometer that is secured with three bolts to the tendon. The relative twist was calculated at each loading step as the difference between the readings of two inclinometers over a distance of 105 mm. To investigate the accuracy of the experimental set up, initial torsion tests were carried out on a steel rod with a diameter of 4.76 mm. The experimentally measured modulus was found to deviate from the nominal shear modulus of steel by 1.6-4%. To assess the inherent material variability between CFRP tendons, three unexposed specimens from group C, derived from the same length of the tendon roll, were tested and the shear modulus values were found to vary by 2.5%.

Experimental series

The experimental programme consisting of two test series is summarised in Table 1. The main experimental variables were: specimen type (group C or D), drying time, exposure time, exposure temperature (23°C and/or 60°C), and the effects of repeated testing.

All the specimens had been previously stored in lab conditions and dried in an oven at 60°C prior to exposure. In series I, the specimens were dried for 2 years. However, after 204 days a mass loss of up to 0.54% for groups C and 0.58% for group D was recorded and thereafter no further mass loss was observed. At the end of the drying period, no cracks or discolouration were visually observed, so we assume no thermo-oxidative ageing effects took place. For series II, the specimens were dried for only 4 months but the mass was found to differ by about 0.10% from series I. In the following discussion, the drying period is not taken as a differentiator.

Control specimens (C-II-3 and D-I-7) were used to measure the baseline dry shear modulus. For the exposed specimens, a 200 mm central region of the 300 mm long sample was immersed in distilled water. This was to protect the region that will be clamped in the torsion test and avoid a premature failure since CFRPs are susceptible to lateral compression when exposed to humid environments. The majority of the specimens were exposed continuously to either 23°C or 60°C. The exceptions were specimens D-I-9 and C-I-8 which were moved after exposure for 141 days at 23°C to an oven at 60°C under similar immersion conditions. This was done to further investigate the equivalency of the total moisture uptake regardless of exposure temperature.

For all the exposed specimens, the same tendon specimen was tested at two or more different time intervals. But there was a concern that if microcracking occurred during a torsion test at a given time interval, this could then precipitate additional moisture uptake such that a greater stiffness degradation might be observed at the next time interval. A range of comparable specimens were therefore tested such that the second time of testing coincided with the first testing of another specimen at the same exposure time (e.g. C-II-9

to C-II-12 and C-II-4 to C-II-7). Hence, if the shear moduli differed beyond the experimental error range allowing for a degree of material variability, this would indicate that microcracking could play a role. In addition, since the exposure time at first testing also varied, any dependency of the microcracking on moisture uptake could also be ascertained.

Specimens C-I-6 and D-I-6 were the first specimens to be tested and used a torsion test set-up with a slightly different right hand support condition. C-I-6 also used a flat plate clamping system which was subsequently changed since there were signs of damage in the clamping region near the exposed area after testing at 112 days. The clamping system used in all the other tests had a curved profile (see Figure 1c) that provided a more uniform radial stress distribution.

The aim was to ensure that under the applied torsional stress, the tendons remained in the elastic range. Based on research work by Hancox (1972) on unidirectional CFRP bars and Ogasawara et al. (2007) who studied unidirectional CFRP laminates, the maximum values of torsion shear stresses τ in the elastic range were 24 and 32 MPa respectively. Failure trial tests on group C specimens showed a linear relationship up to approximately 31 MPa. In the experimental procedure, group C specimens were loaded up to maximum total weight of 200 g whereas a maximum of 250 g was used for group D. The theoretical maximum values of τ at the maximum loading are 21 MPa for group C and 13 MPa for group D so should remain in the elastic range.

Results and Discussion

Optical Microscopy

Figure 2a shows a section of a group C sample at a magnification of 1000 μm. The percentage of voids is significant and extends to long interconnected regions within the resin matrix with a length up to 500 μm and width in the order of 20-30 μm (Figure 2b). Furthermore, a region of different morphology is observed that is characterised by a dense distribution of smaller fibre sizes (Figure 2c, 2d). Similar findings have also been reported in commercially available GFRP tendons by Davalos et al. (2008). Optical microscope pictures for Group D samples reveal a solid matrix distribution and a uniform size of fibres as shown in Figures 3a & b. The only abnormalities are small areas of different 'glassy' morphology (Figures 3 c and d) that have also been observed in group C. This is more pronounced in Figure 3d, where a dark field is applied for comparison. This might be indicative of a two-phase morphology with phases of lower crosslinked structure in the order of 10-20 μm. Soft phases of lower crosslinked structure have been reported by Vanlandingham et al. (1999a) in Atomic Force Microscope pictures of stoichiometric compositions of high crosslink density Epoxy EPON-828 and PACM 20.

DMA tests

Figure 4 illustrates the storage modulus E´ and tanδ values with respect to temperature. The DMA tests yielded $T_{g\text{-}tan\delta}$=163 and 170°C for the two group C samples and $T_{g\text{-}tan\delta}$=147°C for the group D specimen. The higher group C T_g values would suggest a higher crosslink density. This is contradictory to what was expected, since group D was additionally heated during production when the sand coating was applied. Although an increase in T_g values due to post-curing has been reported elsewhere (Wu 1992) this is not

observed here and the group D specimens have a T_g which is 15°C lower than group C. However, group D has a higher absolute peak tanδ value and a narrow α-relaxation that is indicative of a higher crosslink density (Meyer et al. 1995). In group C the tanδ vs temperature plot has a wider α-relaxation that is shifted to higher temperatures resulting in higher T_g values. Meyer et al. (1995) observed a slight increase in width of α- relaxation in connection with lower $T_{g\text{-}tan\delta}$ values in epoxy rich samples that exhibited lower crosslink density. Furthermore, the sample C1 exhibits a small relaxation phase in the range of 60°C-80°C. This phase is denoted as the ω-relaxation phase for the purposes of this paper. A ω-relaxation phase at lower temperature ranges has been reported elsewhere (Meyer et al. 1995; Cavaille et al. 1987) and attributed to a lower crosslink density structure with two phase morphologies in epoxy systems. It is not yet possible to conclude whether this is the case for group C. The relaxation phase might also be indicative of moisture evaporation acting as a plasticising agent but it is not observed in group D. The presence of voids in group C could affect the results, although a lower storage modulus would be expected.

Moisture Absorption

The average mass uptake readings due to exposure in distilled water at 23°C and 60°C for Group C and D are illustrated in Figure 5. The mass uptake behaviour is characterised by a high initial rate that decreases progressively with immersion time. For both temperatures, the group C specimens exhibit a greater mass uptake than the group D specimens at a given time. Both specimen groups concurrently reached the saturation point after approximately 250 days at 60°C. The saturation point at 23°C cannot be clearly identified for either group even after nearly 2 years of exposure and longer exposure times will be required to clarify if the 23°C specimens approach the same mass at saturation, M_{sat}, measured at 60°C. Many researchers argue that M_{sat} depends only on the RH levels and

should be constant irrespective of the accelerated ageing temperature (Diamant et al. 1981; Marais et al. 2000; Papanicolaou et al. 2006). Wright (1981) suggests a small correlation between M_{sat} and temperature, whereas increased M_{sat} values at elevated temperatures have been attributed to either exposure at temperatures close to the wet T_g value (Robert et al. 2010) or weakening of the fibre matrix interface (Davies et al. 1996).

For comparison purposes, Fickian models have been plotted on Figure 5 for each tendon group and exposure temperature. Fickian diffusion is based on the principle of the random motion of molecules. In long cylinders the radial diffusion governs and by integrating the concentration gradient of the solution along the radius of the specimen, Fick's laws can be expressed in terms of mass uptake (Crank 1975):

$$\frac{M_t}{M_{sat}} = 1 - \sum_{n=1}^{\infty} \frac{4}{a^2 a_n^2} \exp(-D a_n^2 t) \quad (1)$$

where M_t is the mass uptake at time t, M_{sat} is the mass uptake at the saturation level, a is the radius of the cylindrical specimen, a_n are the roots of zero Bessel function and D is the diffusion coefficient.

The Fickian process is dependent on two inherent material variables; M_{sat} and the diffusion rate D. The most common method to calculate the diffusion rate is to calculate the gradient of the experimental mass uptake M_t versus $\sqrt{t}$ plot, and substitute into the equation:

$$\frac{M_t}{M_{sat}} = \frac{4}{\sqrt{\pi}} \left(\frac{Dt}{a^2}\right)^{1/2} \quad (2)$$

However, Crank (1975) noted that the simplified form of equation (1) represented by equation (2) is more valid, when $M_t \leq 0.6 M_{sat}$ and is not as robust for cylinders as for the equivalent expression for plane sheets. Therefore, in this study an iterative process was implemented to find the diffusion coefficient by using the immersion time and the

respective mass uptake reading M_t as input variables. One problem is that the mass at saturation M_{sat} and D are interrelated and the selected value of M_{sat} at 23°C is a source of uncertainty, since saturation may not yet have been reached. Adopting as M_{sat} the latest mass uptake reading at 23°C (M_{sat}=1.43% and M_{sat}=1.00% for groups C and D respectively after $\approx$670 days) and 60°C (M_{sat} =2.1% for group C and M_{sat} =1.3% for group D after $\approx$400 days), the derived diffusion rates are $D = 4.04\times10^{-10} \pm 6.72\times10^{-11}$ cm^2/sec and $D = 4.18\times10^{-10} \pm 8.15\times10^{-11}$ cm^2/sec at 23°C, and $D = 1.57\times10^{-09} \pm 5.61\times10^{-10}$ cm^2/sec and $D = 2.18\times10^{-09} \pm 1.63\times10^{-10}$ cm^2/sec at 60°C for groups C and D respectively. If instead it is assumed that the M_{sat} values at 23°C reach the corresponding saturation levels obtained at 60°C, the average diffusivities at 23°C are then $D = 1.38\times10^{-10} \pm 2.40\times10^{-11}$ cm^2/sec and $D = 2.16\times10^{-10} \pm 2.16\times10^{-11}$ cm^2/sec for group C and D respectively and display a lower standard deviation. These latter values will be used in all subsequent calculations relating to the 23°C behaviour and the related Fickian model predications are plotted in Figure 5. The Fickian model predictions agree well with the experimental data. The group D specimens have a solid matrix with no voids and are more likely to comply with Fick's laws assumptions. However, in spite of the high void content observed in the group C optical microscopy photos, the mass uptake behaviour generally agrees with the Fickian model although a small divergence between the Fickian model and the experimental data can be observed for group C at 60°C for exposure between 70 and 154 days. The group C experimental data has a greater standard deviation when compared with Group D. Although the group C samples have higher M_{sat} values, they have lower average diffusivity values. Despite the inconclusive DMA test results on the additional heating effect in group D, Krishna et al. (2010) reported decreased values of M_{sat} with increased post-cure (increase of curing time and temperature) for

glass/epoxy specimens, whereas the diffusivity values and the time of saturation point were similar. The mass uptake rate in group C during the early exposure times is higher than in group D and gradually drops to lower values. This behaviour might indicate the synergistic effects of voids and a two phase structure, where a lower crosslink density with a higher free volume dominates during the initial exposure times. Vanlandingham et al. (1999b) contended that the free volume is the governing factor in the moisture absorption mechanism in epoxy-amine systems. Regardless of any crosslinking, the extent of the voids in group C would be expected to dominate the mass uptake behaviour.

Torsion tests

The exposed specimens were removed from solution and tested within an hour. To determine the extent of evaporation between exposure and testing, trial specimens that had been exposed at 23°C for 119 days were left to dry in lab conditions. After an hour, a maximum mass loss of 0.0065% and 0.004% was measured for Groups C and D respectively. So the influence of evaporation was not felt to be significant.

For each torsion experiment, three load-unload cycles were carried out. For each load cycle the graph of the torque versus twist was drawn and the shear modulus was back-calculated from the gradient of the linear best fit line. The shear modulus was taken as the average from the three load cycles. The unloading steps were also recorded as the weights were gradually removed. Figure 6 shows the load-unload curves of a dried and saturated specimen from C-II series. The loading behaviour can be approximated as linear-elastic although some non-linearity is observed in the saturated specimen and attributed to the softening of the matrix. The hysteresis in the unloading curve was found to increase with exposure time.

The measured torsional shear modulus of the group C and D CFRP tendons exposed in distilled water at either 23°C or 60°C, can be seen in Figure 7. In this figure, the predicted Fickian mass uptake was calculated for each exposure time and plotted. Group C and D have different diffusion coefficient values and therefore have different mass uptake values for the same exposure time. The error bars plotted correspond to one standard deviation representing the variation between the three experimental load runs.

The dried shear modulus for group D-I is G_o= 5.91 GPa, whereas the dried shear modulus for group C-II is G_o= 5.19 GPa, which is 12% lower. Groups C and D have the same epoxy, fibre type and fibre volume, so this deviation is attributed primarily to the void content in group C. For both groups the shear modulus decreased with moisture ingression but the reduction was greater for Group C. A 17% decrease in shear modulus for the group D specimens (D-I-9 sample) is observed after 141 days of exposure at 23°C plus 71 days of exposure at 60°C. This exposure regime is equivalent to 1.05% moisture absorption. A drop of around 29% is observed in group C (C-I-8 sample) for the same exposure conditions and exposure time period that corresponds to a higher mass uptake M_t =1.77%. By defining the shear modulus degradation as G_t/G_o, the results for groups C and D for similar mass uptakes are listed in the Table 2. Even for a given percentage of M_t/M_{sat}, Group C shows a somewhat greater degradation than group D and again this is attributed to the voids and differences in the production process. Note that for similar mass uptakes the C-I-6 specimen shows a greater degradation than C-II-4 and -5 perhaps due to microcracking in the clamping region with the flat profile clamps. As discussed, this phenomenon was avoided in subsequent tests by changing the clamping system.

For the C-II specimens exposed at 60°C the shear modulus appears to reduce gradually at around 3.70 GPa for M_{sat}=2.1% and it is deduced there exists a shear modulus at saturation

G_{sat} (as illustrated in Figure 10). This phenomenon is attributed to the softening of the matrix material. The shear modulus at the saturation point is not clearly defined in group D-I but it seems to approach G= 4.94 GPa for M_t=1.05%. The G_{sat} values will be verified for both groups by testing further a CFRP specimen, when full saturation at 23°C is reached.

Specimens in the C-II series with the same predicted mass uptakes after exposure at either 23°C or 60°C exhibit similar shear moduli values. This consistency generates confidence in the 60°C accelerated ageing process and suggests the higher temperature does not exacerbate any material deterioration. Insignificant changes in shear moduli are observed in the C-II specimens with the same Fickian mass uptakes, regardless of whether that time point represented the first or second time of testing. Consequently, it can be inferred that, within the experimental load range, there is a negligible correlation between any microcracking from repetitive testing and subsequent degradation mechanisms in the epoxy material.

Prediction model

Design models have been developed to predict the mechanical degradation behaviour of FRPs due to exposure in wet environments. However, the main focus tends to be on fibre dominated properties. The formulations described here (Papanicolaou et al. 2006; Phani and Bose 1987; Chen et al. 2007b) include an exponential term that potentially reflects the exponential Fickian mass uptake behaviour. The substantive difference between the models lies in the value of the exponential term that represents the rate of mechanical degradation.

Phani and Bose (1987) studied E-glass Chopped Strand Mat (CSM) laminates HSR 8131 (Bakelite Hylam Ltd, India) under hygrothermal conditions and showed that the flexural strength can be expressed as:

$$\sigma(t) = (\sigma_O - \sigma_\infty)\exp(-t/\tau) + \sigma_\infty \quad (3)$$

Where $\sigma(t)$ is the flexural strength at exposure time t, σ_o and σ_∞ are the flexural strength at zero and infinite time respectively and τ is a time variable that increases with increasing temperature according to:

$$1/\tau = 1/\tau_O \exp(-E_a/RT) \quad (4)$$

where E_a is the activation energy, R is the Universal gas constant and T is the temperature in Kelvin. Chen et al. (2007b) studied the long-term durability of glass FRP bars in concrete pore solution and assumed a total loss of the tensile strength at infinite time by adopting the relationship:

$$Y = 100\exp(-t/\tau) \quad (5)$$

where Y is the tensile strength retention (%), t is the exposure time, τ is $1/k$ and k is the degradation rate. Consequently, the steepness of the exponential curve is a function of the degradation rate k. However, equation 5 was developed for glass FRP bars with a polyester matrix where the matrix decomposes under longer exposure times and at higher temperatures, and the glass fibres leach out. A generic model to describe the mechanical degradation in different types of unreinforced polymers was proposed by Papanicolaou et al. (2006) and called the RPM model

$$\frac{P_t}{P_O} = s + (1-s)\exp(-sM_t) \quad (6)$$

where P_t represents the mechanical property at exposure time t, M_t is the percentage mass uptake at exposure time t and $s=P_\infty/P_o$ at the saturation point. The model was applied to

epoxy specimens exposed in distilled water at 60°C and 80°C and tested in 3 point bending (Papanicolaou et al. 2006).

The RPM model was used to predict the expected shear stiffness at a given time and compared with the experimental findings for groups C and D in Figure 8. The RPM input degradation rates of 0.709 and 0.836 were found using $s = G_{sat}/G_o$ as derived from the latest experimental data for group C and D respectively. The RPM model seems to agree better with the experimental findings of groups C-II series than with group D. However, for both groups the predictions tend to deviate near the saturation point. One issue in this calculation is that the degradation ratio is assumed to be the same throughout the bulk of the tendon. Yet in practice the conditions in a torsion test are not uniform since the moisture diffuses inwards from the outer tendon surface and the torsional contribution of a given annulus depends on the distance from the centre of the tendon.

To more accurately reflect these details, a predictive model was developed to relate the diffusion process through the cross-section of the CFRP specimens and the shear stiffness degradation mechanism. It is assumed that, as the solution ingress proceeds from the outer tendon surface towards the centre of the cross-section, the shear stiffness of the 'degraded' regions (outermost regions) is decreased by a certain factor that is dependent on the moisture concentration C. At full saturation a residual stiffness G_{sat} remains. The model is based on the Fickian diffusion process. The solution procedure is as follows:

- The tendon radius is discretised to a series of n rings (taken as n=200 in the current work) and the concentration profile along the radius is calculated (see Figure 9a). The concentration profile is derived in terms of percentage moisture concentration by assuming that the solution at the tendon surface has a concentration equal to 1.00.

- The average concentration value of each ring for the specific time point is calculated as:

$$Cavi = (C_i + C_{i+1}) / 2 \quad (7)$$

and is assumed to be constant over the area of the segment.

- The shear stiffness of each ring ΔG_i which is over and above G_{sat} is defined as:

$$\Delta G_i = (1\text{-}Cavi) \cdot (G_o - G_{sat}) \quad (8)$$

where G_o is the shear modulus of the tendon in the dry condition, G_{sat} is the shear modulus of the tendon at saturation and *Cavi* is the average concentration of the segment. The $(G_o\text{-}G_{sat})$ component reflects the degradation of the matrix component due to moisture uptake between t=0 and t= ∞. The (1-*Cavi*) is a degradation factor based on the concentration of the solution and when a region is fully saturated *Cavi*=1.00.

- The ΔG_i values are integrated across the section according to the polar second moment of area J as derived by the torsion shear stress distribution across the section (Equation 9).The polar second moment of area for a cylindrical annulus with an inner radius r_i and outer radius r_{i+1}, is denoted as J_i. When the shear stiffness values of the annuli vary with moisture uptake e.g. equation 8, then the equivalent averaged contribution to the overall tendon shear stiffness ΔG_{eq} above G_{sat} can be defined as:

$$\Delta G_{eq} = \frac{\sum_{i=1}^{n} \Delta G_i J_i}{J} \quad (9)$$

where $J_i = \pi(r_{i+1}^4 - r_i^4) / 2$ and J is the polar second moment of area of the solid tendon.

- The resulting G_t value for the tendon after exposure time t is then:

$$G_t = G_{sat} + \frac{\sum_{i=1}^{n} (1\text{-}Cavi) J_i}{J} (G_o - G_{sat}) \quad \text{(see Figure 9b)} \quad (10)$$

subject to the following boundary conditions: as t → 0, G_t=G_o and as t→ ∞, G_t=G_{sat}.

Figure 10 illustrates the comparison between the experimental data and the prediction models for both groups C and D. To plot the shear modulus versus the exposure time it was necessary to use a common baseline for the 23°C and the accelerated 60°C results. The time axis in Figure 10 therefore corresponds to exposure at 23°C and so time shift factors were applied for the specimens exposed at 60°C to convert these readings to equivalent exposure times at 23°C. The time shift factors were calculated as the ratio of mass uptake rate at 60°C to the respective one at 23°C at specific exposure times leading to factors of 12 and 10 for group C and D respectively. The prediction model seems to underpredict the shear modulus values for the initial exposure times up to 141 days for both groups C and D, but generally captures the trend of the experimental findings.

Implications and further developments

The full immersion of the CFRP tendons results in direct contact with water whereas in CFRP prestressed concrete the concrete cover will offer a protective casing to the tendons. Hence, the exposure conditions in the current work could be rather onerous compared with what might be expected in practice. A loss of matrix stiffness over time will have implications for matrix-dominated properties such as the bond behaviour of CFRP tendons in concrete. This will be of particular relevance in cases where the outer resin rich layer of the tendon surface is a major contributor to the bond resistance. A study on the long-term durability of bond strength between CFRP tendons and concrete is on-going.

Conclusions

The mass uptake and torsional stiffness behaviour over exposure time of two tendon groups C and D with the same material characteristics (epoxy, fibre type, fibre volume) but

different production processes were investigated. The Group C tendons were uncoated whereas Group D samples were sand coated and so were subjected to additional curing to affix the sand particles to an outer resin layer. The T_g values measured using DMA tests were inconclusive in terms of identifying differences in the crosslink density between groups C and D. Group C tendons immersed in water exhibited a 60% greater mass uptake at saturation than group D. This was primarily attributed to the presence of voids, as observed in the optical microscope pictures. Torsion test results show that the shear stiffness of the CFRP tendon specimens immersed in distilled water degrades with time. For the group C specimens a 29% decrease in the shear modulus was measured after 325 days of exposure at 60°C (C-II series) and by this time the tendons appeared to have reached saturation. For group D the reduction in stiffness was lower, 17%, and this was attributed to the lower moisture uptake rate. However, further testing is required to confirm the group D shear modulus at saturation. The use of 60°C as an accelerated temperature did not appear to induce additional degradation even at longer exposure times. A prediction model that relates the time-dependent radial diffusion through a CFRP tendon and the shear modulus contribution from each segment in a discretised section was proposed. The model generally showed good agreement with the experimental findings for both groups C and D.

Acknowledgements

We are grateful to SACAC for their technical and financial support. We also appreciate the financial support from the Onassis Foundation.

References

Abanilla, M.A, Karbhari, V.M. and Li, Y. (2006). "Interlaminar and intralaminar durability characterization of wet layup carbon/epoxy used in external strengthening." *Composites Part B*, 37(7-8), 650-661.

ACI 440.1-R06 (2006). Guide for the design and construction of concrete reinforced with FRP bars. American Concrete Institute, Farmington Hills, MI, USA.

Adamson, M.J. (1980). "Thermal expansion and swelling of cured epoxy resin used in graphite/epoxy composite materials." *J. Mater. Sci.*, 15(7), 1736-1745.

Ankara, A., Weisgerber, D. and Vilsmeier, J. (1986). "Effect of post-curing on properties of carbon fibre-epoxy composites." *Mater. Sci. Technol*., 2(7), 647-651.

ASTM. (2008). "Standard test method for shear modulus at room temperature." ASTM E143-02, West Conshohocken, PA.

Birger, S., Moshonov, A. and Kenig, S. (1989). "The effects of thermal and hygrothermal ageing on the failure mechanisms of graphite-fabric epoxy composites subjected to flexural loading." *Composites*, 20(4), 341–348.

Burgoyne, C. and Balafas, I. (2007). "Why is FRP not a financial success?" *Proc., FRPRCS-8: 8th Int. Symp. on FRPs for Reinforced Concrete Structures*, edited by T. Triantafillou, University of Patras, Greece, 16-18 July, 1-10.

Cavaille, J.Y., Johari, G.P. and Mikolajczak, G. (1987). "Dynamic mechanical properties of structural glass fibre-epoxy composites." *Polymer*, 28(11), 1841-1846.

Chen, Y., Davalos, J.F., Ray, I. and Kim, H.Y. (2007a). "Accelerated Aging Tests for Evaluations of Durability Performance of FRP Reinforcing Bars for Concrete Structures." *Compos. Struct*., 78(1), 101-111.

Chen, Y., Davalos, J.F. and Ray, I. (2007b). "Durability prediction for GFRP reinforcing bars using short-term data of accelerated aging tests." *J. Compos. Constr*., 10(4), 279-286.

Crank, J. (1975). *The mathematics of diffusion.* Clarendon Press, Oxford, UK.

Davalos, J.F, Chen, Y. and Ray, I. (2008). "Effect of FRP bar degradation on interface bond with high strength concrete." *Cement and Concrete Composites*, 30(8), 722-730.

Davies, P., Pomies, F. and Carlsson, L.A. (1996). "Influence of water and accelerated aging on the shear fracture properties of glass/epoxy composite." *Appl. Compos. Mater.*, 3(2), 71-87.

Diamant, Y., Marom, G. and Broutman, L. (1981). "The effect of network structure on moisture absorption of epoxy resins." *J. Appl. Polym. Sci.*, 26(9), 3015-3025.

Dolan, C.W., Ahearn, E.B, Deng, J., Tanner, J.E. and Mukai, D. (2008). "Durability and accelerated ageing testing of CFRP repair systems." *Proc., CICE 2008: 4th International Conference on FRP Composite in Civil Engineering*, edited by Masoud Motavalli, Zürich, Switzerland, 22-24 July, 22–24.

Hancox, N.L. (1972). "The use of a torsion machine to measure the shear strength and modulus of unidirectional carbon fibre reinforced plastics." *Mater. Sci.,* 7(9), 1030-1036.

Hancox, N.L. (1977). "The effects of flaws and voids on the shear properties of CFRP." *J. Mater. Sci.,* 12(5), 884-892.

Hartt, W. H. and Venugopalan, S. (2002). "Corrosion evaluation of post-tensioned tendons on the Mid Bay Bridge in Destin, Florida." *Florida Department of Transportation Research Center report 33890.*

Hiermer, T., Schmitt-Thomas, Kh.G. and Yang, Z.G. (1998). "Mechanical properties and failure behaviour of cylindrical CFRP-implant-rods under torsion load." *Composites Part A,* 29(11), 1453-1461.

Huang, H. and Talreja, R. (2005). "Effects of void geometry in elastic properties of unidirectional fiber reinforced composites." *Compos. Sci. Technol*., 65(13), 1964-1981.

Huang, J. and Aboutaha, R. (2010). "Environmental reduction factors for GFRP bars used as concrete reinforcement: New Scientific Approach." *J. Compo. Constr.*, 14(5), 479-486.

Kelly, A. (1989). "Thermosetting Resin Matrices." *Concise encyclopedia of composite materials*, The Pergamon Press, Oxford, UK, 267.

Krishna, R., Revathi, A., Srihari, S. and Rao, R. (2010). "Post-curing effects on hygrothermal behavior of RT-cured glass/epoxy composites." *J. Reinf. Plast. Compos.*, 29(3), 325-330.

Lam, Y.C., Li, J. and Joshi, S.C. (2003). "Simultaneous optimisation of die-heating and pull-speed in pultrusion of thermosetting composites." *Polym.Compos.*, 24(1), 199–209.

Li, S., Ding, Z., Xu, L., Lee, L.J. and Engelen, H. (2002). "Influence of heat transfer and curing on the quality of pultruded composites. I:Experimental." *Polym.Compos.*, 23(5), 947–956.

Liu, L., Zhang, B.M., Wang, D.F. and Wu, Z.J. (2006). "Effects of cure cycles on void content and mechanical properties of composite laminates." *Compos. Struct.*, 73(3), 303-309.

Lynch, D. (2012). "Hammersmith flyover: returning to full strength" *New Civil Engineer*, 98, 14-16.

Marais, S., Metayer, M., Nguyen, T.Q., Labbe, M. and Saiter, J.M. (2000). "Diffusion and permeation of water through unsaturated polyester resins-influence of resin curing." *Eur. Polym. J.*, 36(3), 453-462.

Mayer, R.M. (1996). "Manufacturing considerations." *Design with reinforced plastics*, Bourne Press, London, UK, 136-138.

Meyer, F., Sanz, G., Eceiza, A., Mondragon, I. and Mijovic, J. (1995). "The effect of stoichiometry and thermal history during cure on structure and properties of epoxy networks." *Polymer*, 36(7), 1407-1414.

Micelli, F. and Nanni, A. (2001). "Issues related to durability of FRP reinforcement for RC structures exposed to accelerated ageing." *Proc., ASC 16th Annual Technical Conference*

(CD-ROM), edited by M.W. Hyer and A.C. Loos, Virginia Tech. University, Blacksburg, VA, 9-12 September, 12pp.

Min, B.G., Hodgkin, J.H. and Stachurski, Z.H. (1993). "The dependence of fracture properties on cure temperature in a DGEBA/DDS epoxy system." *J. Appl. Polym. Sci.*, 48 (7), 1303-1312.

Ogasawara, T., Yokozeki, T., Onta, K. and Ogihara, S. (2007). "Linear and nonlinear torsional behavior of unidirectional CFRP and GFRP." *Compos. Sci. Technol*., 67(15-16), 3457-3464.

Olivier, P., Cottu, J.P. and Ferret, B. (1995). "Effects of cure cycle pressure and voids on some mechanical properties of carbon/epoxy laminates." *Composites*, 26(7), 509–515.

Papanicolaou, G.C., Kosmidou, Th.V., Vatalis, A.S. and Delides, C.G. (2006). "Water absorption mechanism and some anomalous effects on the mechanical and viscoelastic behavior of an epoxy system." *J. Appl. Polym. Sci.*, 99(4), 1328-1339.

Phani, K.K. and Bose, N.R. (1987). "Temperature dependence of hydrothermal ageing of CSM-laminate during water immersion." *Compos. Sci. Technol.*, 29(2), 79-87.

Robert, M., Wang, P., Cousin, P. and Benmokrane, B. (2010). "Temperature as an accelerating factor for long-term durability testing of FRPs: Should there be any limitations?" *J. Compos. Constr*., 14(4), 361-367.

Scott P. and Lees J.M. (2012). "Effect of solution exposure on the combined axial-shear behaviour of unidirectional CFRP rods." *Composites Part A*, 43(9), 1599-1611.

Vanlandingham, M.R., Eduljee, R.F. and Gillespie, J.W. (1999a). "Relationships between stoichiometry, microstructure, and properties for amine-cured epoxies." *J. Appl. Polym. Sci.*, 71(5), 699-712

Vanlandingham, M.R., Eduljee, R.F. and Gillespie, J.W. (1999b). "Moisture diffusion in epoxy systems." *J. Appl. Polym. Sci.*, 71(5), 787-798.

Wright, W. W. (1981). “The effect of diffusion of water into epoxy resins and their carbon-fibre reinforced composites.” *Composites*, 12(3), 201-205.

Wu, C.S. (1992). “Influence of post-curing and temperature effects on bulk density, glass transition and stress-strain behaviour of imidazole-cured epoxy network.” *J. Mater. Sci*., 27(11), 2952–2959.

Xiao, G.Z and Shanahan, M.E.R. (1997). “Water absorption and desorption in an epoxy resin.” *J. Polym. Sci*., 35(16), 2659-2670.

Zhu, H., Li, D., Zhang, D., Wu, B. and Chen, Y. (2009). “Influence of voids on interlaminar shear strength of carbon/epoxy fabric laminates.” *Trans. Nonferrous Met. Soc. China*, 19(2), s470-s475.

Table 1: Exposure programme for C-I and C-II series and D-I-series immersed in distilled water.

Specimen	Exposure temperature (°C)	Exposure time (days)																	
		0	**3**	**7**	**14**	**17**	**27**	**31**	**35**	**63**	**89**	**99**	**104**	**112**	**132**	**141**	**159**	**212**	**325**
D-I-6	23				x[a]				x[a]		x								
D-I-7	Dry	x																	
D-I-9	23/60												x			x	x	x	
C-I-6	23				x[a]				x[a]					x[b]					
C-I-8	23/60															x	x	x	
C-I-9	23													x					
C-II-3	Dry	x																	
C-II-4	23			x			x			x									
C-II-5	23						x			x									
C-II-6	23									x					x				
C-II-7	23														x				
C-II-8	60		x																
C-II-9	60				x	x													
C-II-10	60					x			x										
C-II-11	60								x			x							x
C-II-12	60											x							x

The specimen identification a-b-c denotes a= specimen group C or D; b= experimental series I or II; c= specimen number; x= time of testing; shaded area=exposure at 60°C.

[a] Slightly different torsion test set up

[b] Signs of damage at the clamping area

Table2: Shear modulus degradation for similar mass uptake ratios: Comparison between group C and D.

Specimen	**M_t (%)**	**M_t /M_{sat}**	**G_t / G_o**
C-II-4	0.389	19%	0.96
C-II-5	0.389	19%	0.96
C-I-6	0.440	21%	0.80
D-I-6	0.266	20%	0.99
C-I-8	1.246	59%	0.75
D-I-9	0.729	56%	0.85

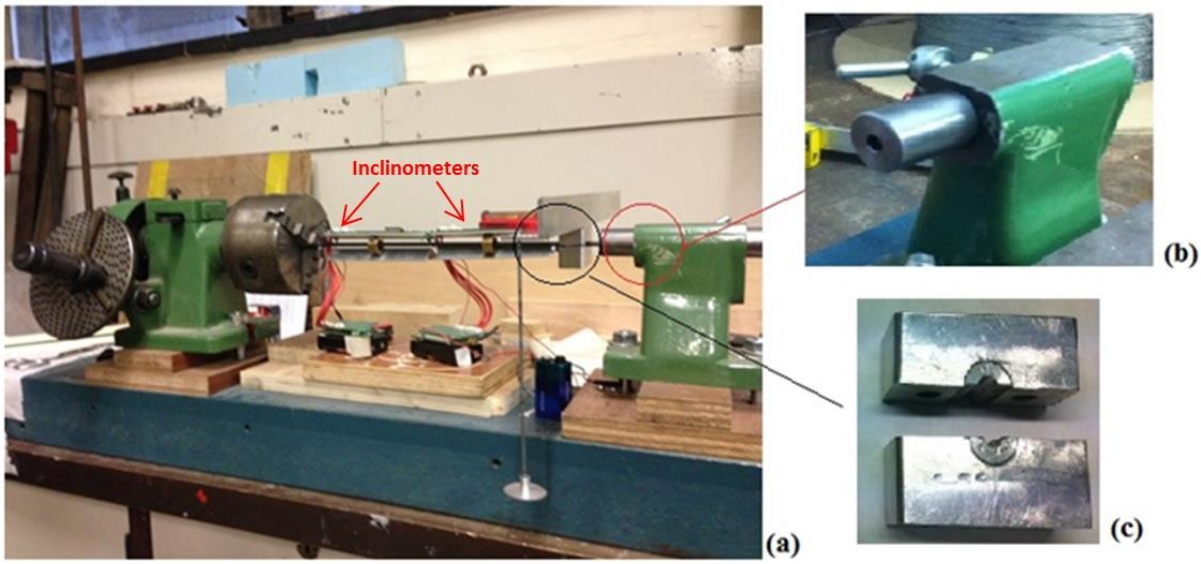

Figure 1. (a) Torsion test set up, b) Axially unrestrained edge and c) Curved clamp.

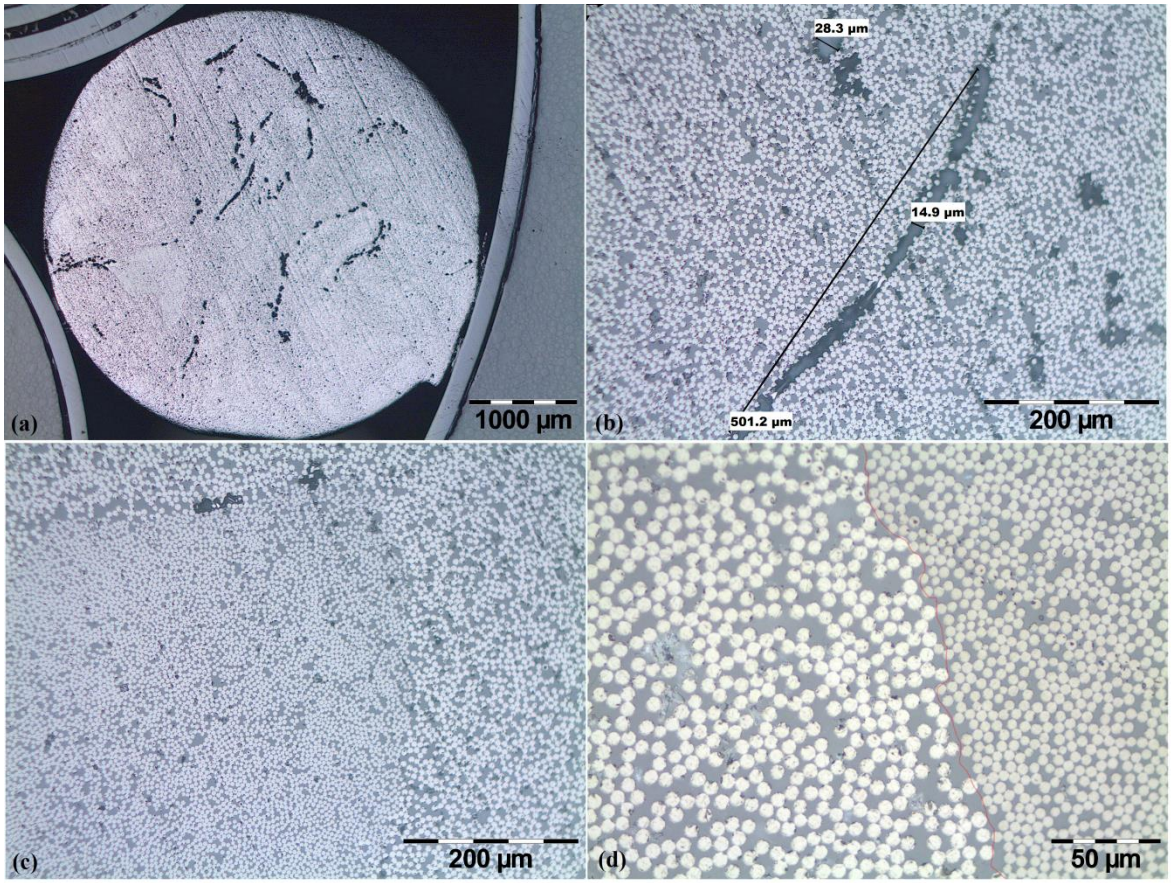

Figure 2. Optical Microscopy: Group C a) 1000 µm, b) void area 200µm, c) 200 µm interfacial region, d) 50 µm interfacial region.

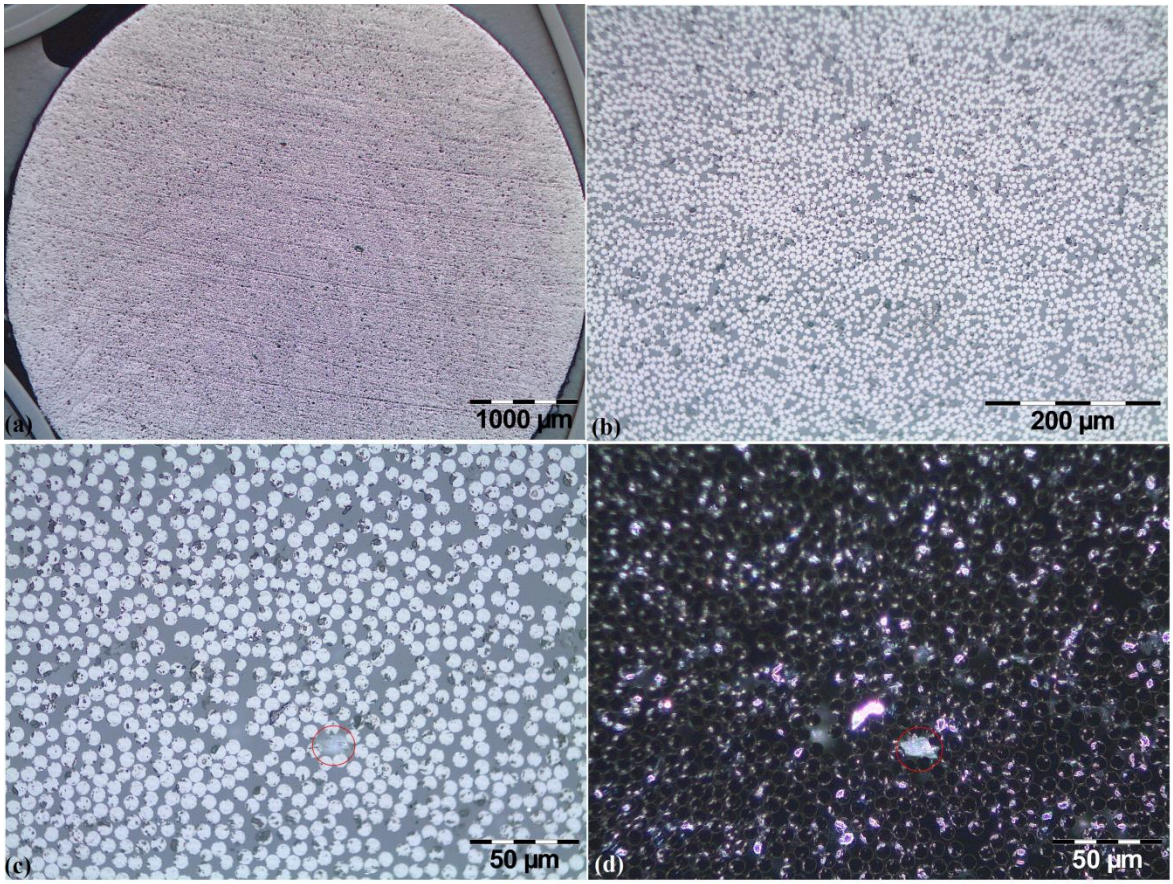

Figure 3. Optical microscopy: Group D a) 1000µm, b) 200 µm, c) 50µm light field and d) 50 µm dark field.

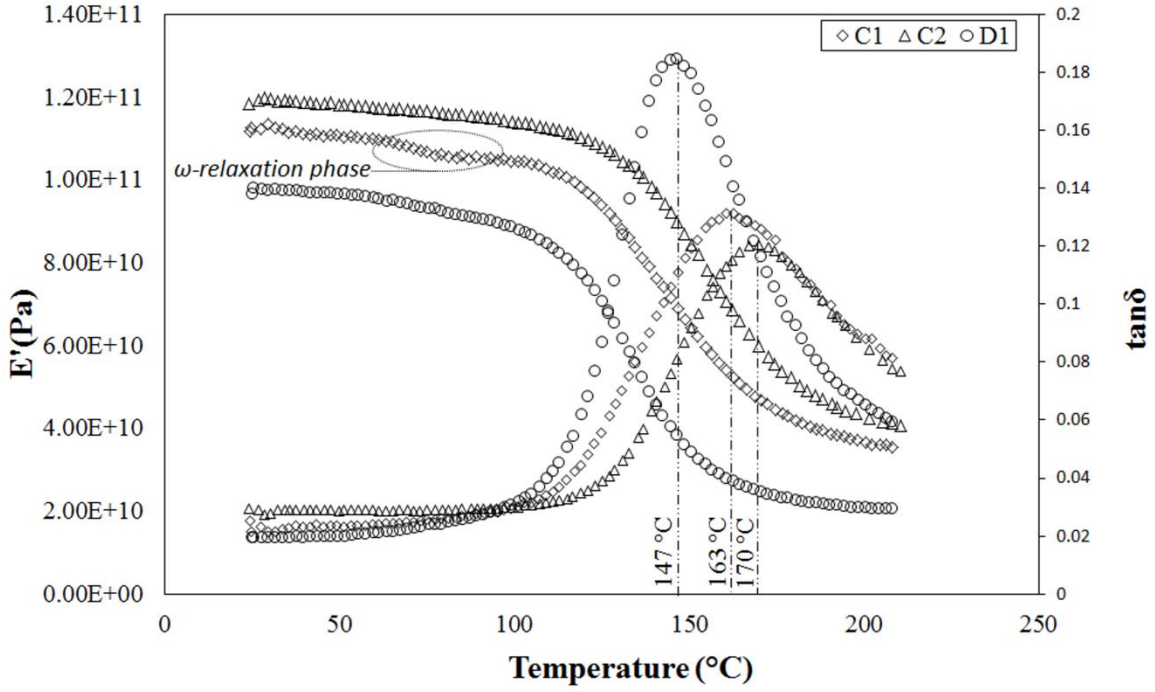

Figure 4. DMA tests group C versus group D.

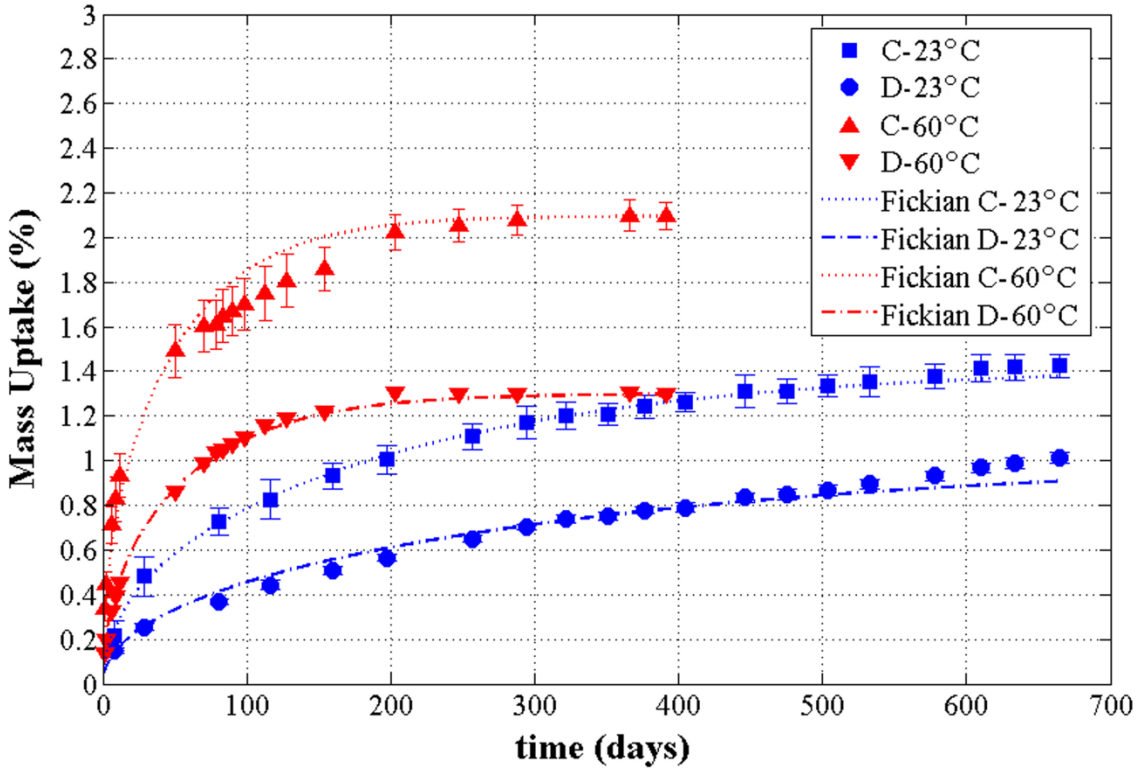

Figure 5. Moisture Uptake in group C and D.

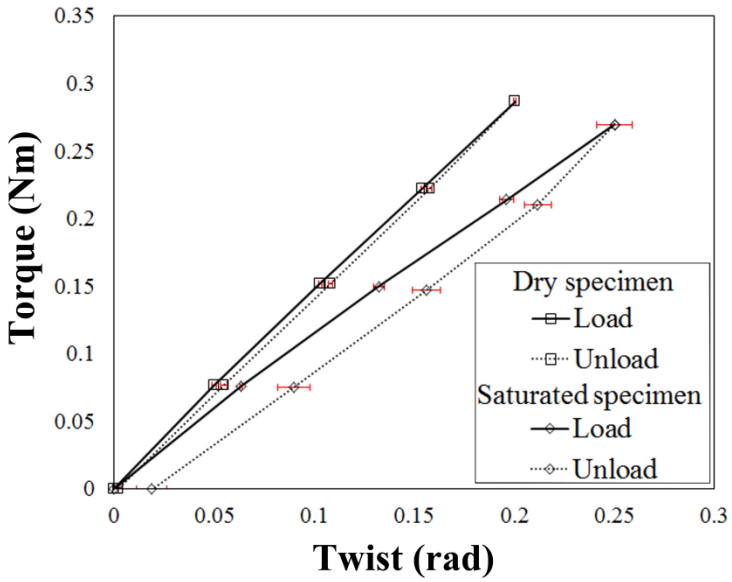

Figure 6. Load-Unload curves for a "dry" specimen, C-II-3, and a "saturated specimen", C-II-12.

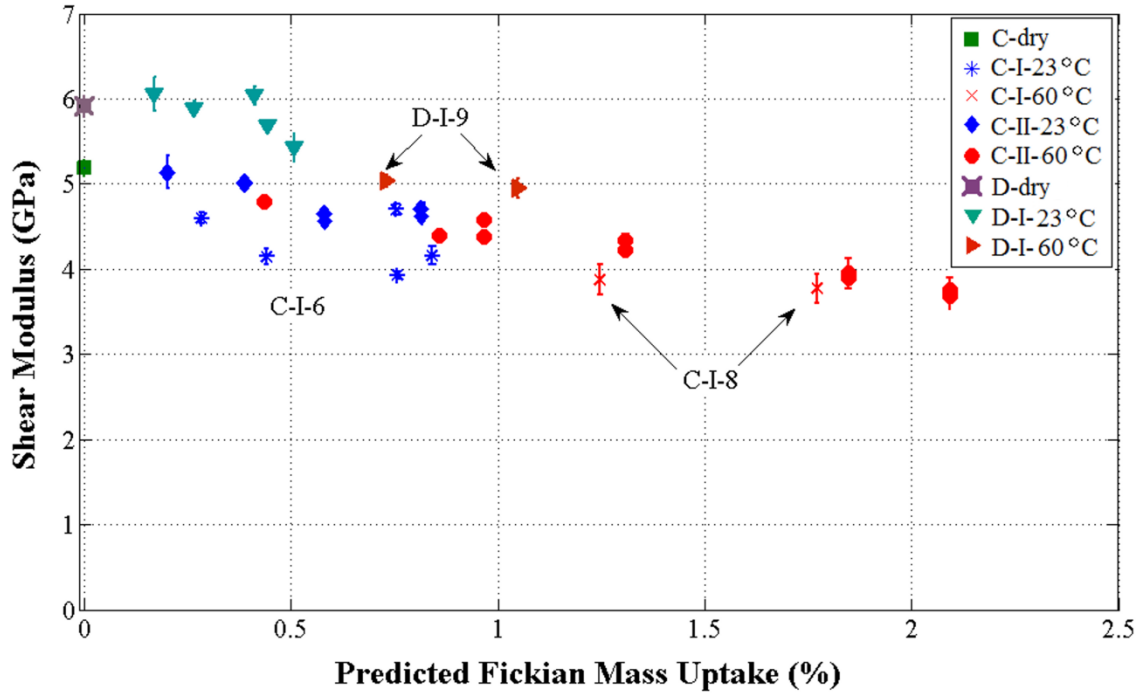

Figure 7. Shear Modulus Degradation with predicted Fickian Mass Uptake: Groups C and D at 23°C and 60°C.

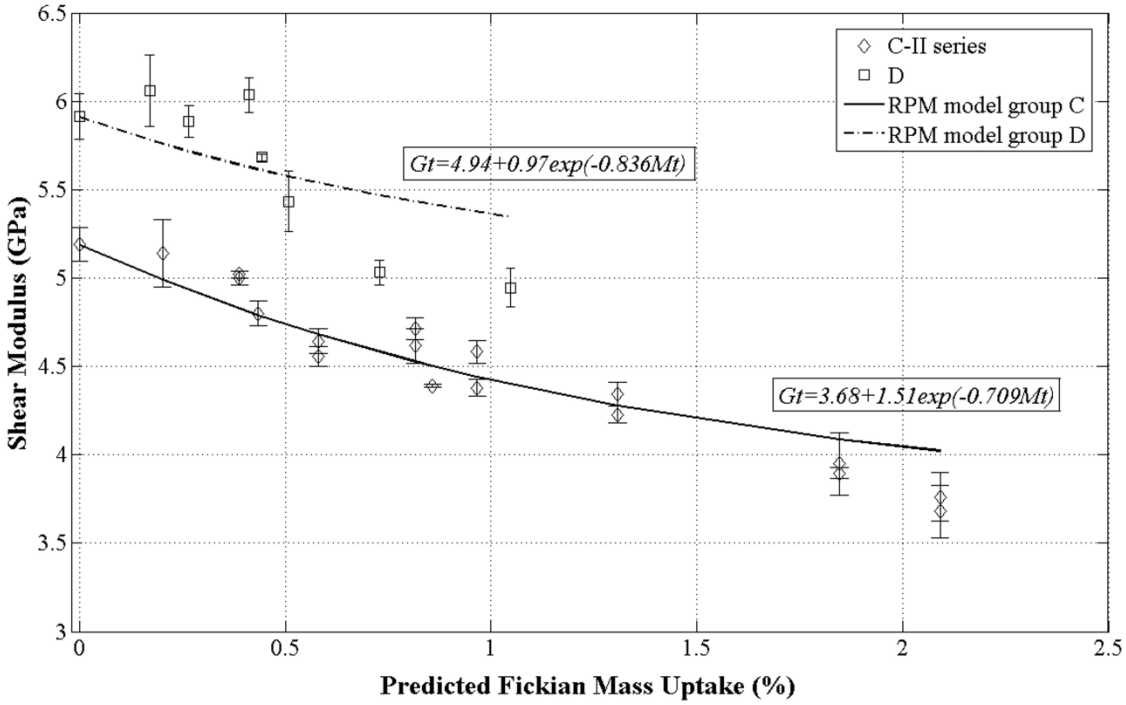

Figure 8. Comparison of RPM model with experimental findings for group C-II and D-I series.

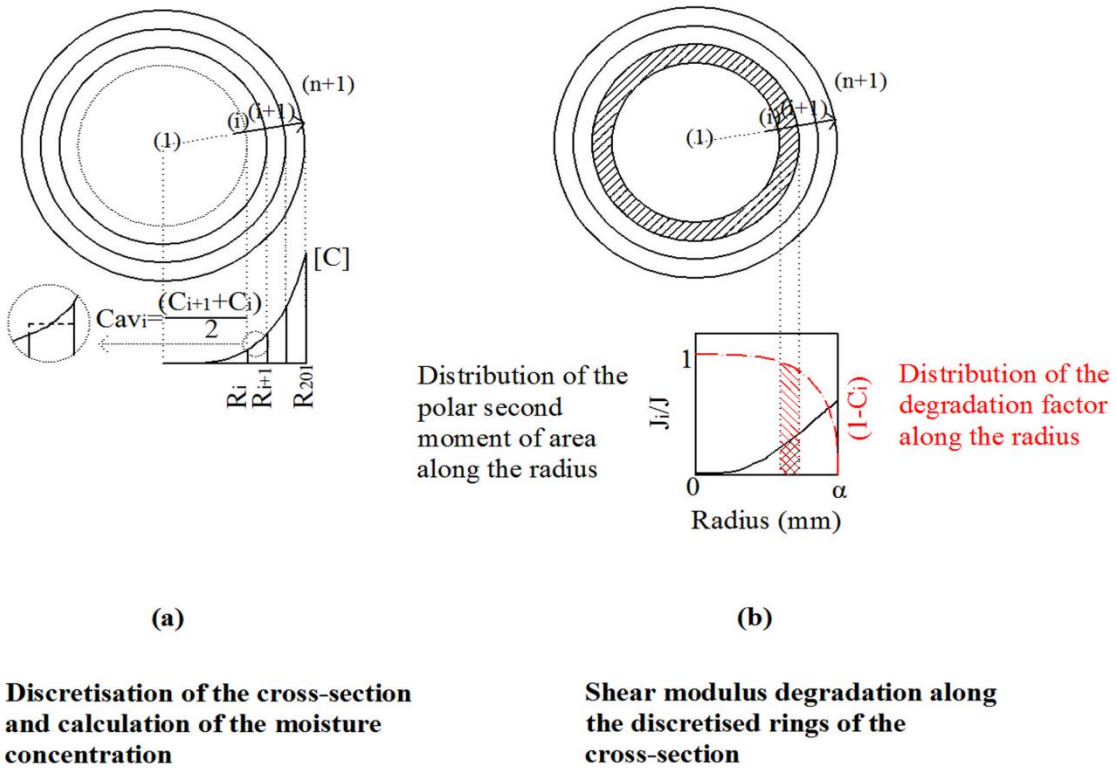

Figure 9. (a) Discretisation of a CFRP tendon section and calculation of the average moisture concentration for each segment, (b) Calculation of the polar second moment of area factor and of the degradation factor for each segment.

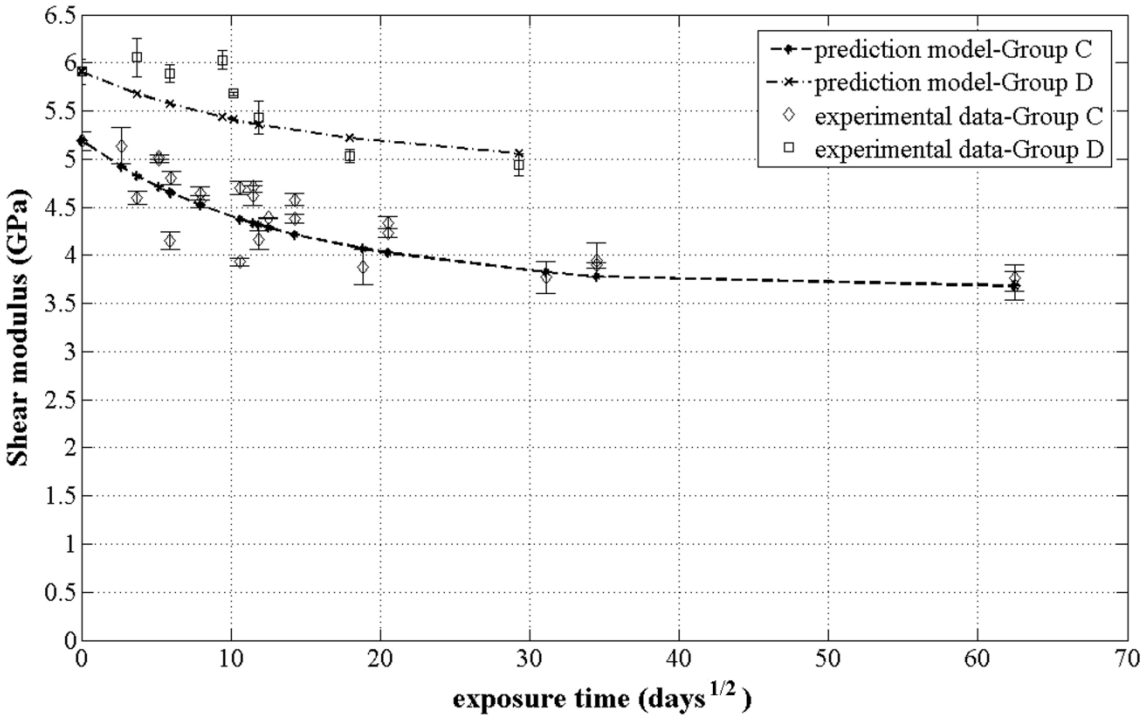

Figure 10. Comparison between the prediction model and the experimental data for groups C-I & II and D-I series.